ACS OMEGA

http://pubs.acs.org/journal/acsodf

Article

Assessment of the Toxicity of Aluminum Oxide and Its Nanoparticles in the Bone Marrow and Liver of Male Mice: Ameliorative Efficacy of Curcumin Nanoparticles

Alshaimaa A. I. Alghriany, Hossam EL-din M. Omar, Amera M. Mahmoud, and Mona M. Atia*

Cite This: *ACS Omega* 2022, 7, 13841−13852

Read Online

ACCESS | Metrics & More | Article Recommendations | Supporting Information

ABSTRACT: The potential influence of nanoparticles (NPs) on the liver and bone marrow has received attention. The aim of this work was to evaluate the effect of nanocurcumin on the oxidative stress, apoptosis, and toxicity induced by Al_2O_3 and its NPs. The experimental animals (n = 72 mice) were divided into the following groups: group I, as a control; groups II and III, as aluminum oxide and its NPs (6 mg/kg); group IV, as aluminum oxide + nanocurcumin (Al_2O_3 + N-Cur, 20 mg/kg); and group V, as aluminum oxide NPs + nanocurcumin (Al_2O_3-NP + N.Cur., 20 mg/kg). Al_2O_3 and its NP groups significantly increased p53, Nrf2 levels, and the white blood cell count. They also decreased the Hsp70 level, antitrypsin, immunoglobulin G, and the red blood cell count. In addition, they significantly decreased the total and differential bone marrow cell counts and the maturation index ratio (MIR). Nanocurcumin (N.Cur.) reverted the previous proteins, blood parameters, total bone marrow cell count, and the MIR as M/E, I/Mg, MMI, I/Me, and EMI to normal. Furthermore, N.Cur. prevented apoptosis and reduced the histopathological score and collagen fiber percentage caused by Al_2O_3 and its NPs in the liver. Nanotechnology was used to increase the therapeutic efficiency of curcumin against the harmful effects of oxidative stress associated with Al_2O_3 NPs.

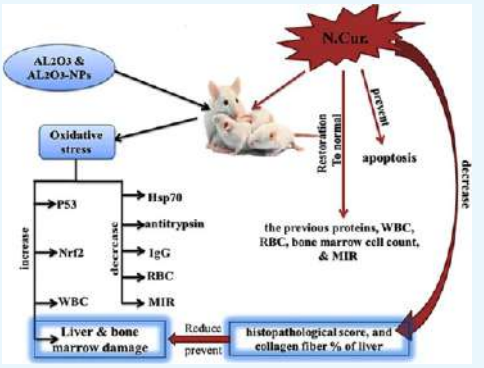

1. INTRODUCTION

Simple metal oxides, such as aluminum oxide (Al_2O_3), are the most commercially important nanoparticles (NPs). The micro- and nanoscale forms of aluminum (Al) exhibit excellent lightness, mechanical resistance, and strong oxidizing power. Al microparticles and Al-NPs have been used in the industry, including food products, because of their distinctive qualities.[1,2] The properties of NPs, such as size, shape, surface charge, and porosity, are intimately connected with functionality and their effects on health and the environment.[3] NPs exhibit exclusive physicochemical properties according to the manufacturing processes, even with the raw materials being the same. Moreover, NPs elicit toxicities that differ from that of naturally occurring particles due to their smaller size, larger surface area, high reactivity, and greater ability to cross biological barriers, and their properties can be altered in biological conditions.[4,5]

Experimental conditions, such as dose, time, and route of exposure, influence the toxicity and distribution of NPs to the organs. In addition, NPs can be trapped by macrophages and remain in the spleen and liver for a long time.[6] Animals uptake NPs through dermal, oral, and respiratory routes,[7] where they may exhibit toxicity ranging from direct impacts on their metabolisms, protein structure, and its expression.[8] It has been reported that Al_2O_3-NPs triggers the production of reactive oxygen species (ROS), pro-inflammatory cytokines, and DNA mutations that result in substantial damage to the brain, liver, kidneys, and the immune system.[9]

In addition, Al_2O_3-NP exposure can cause genetic damage, inflammatory responses, carcinogenicity, cytotoxicity, and mitochondrial dysfunction.[10] Aluminum spreads throughout the body following oral intake, with buildup in the bone, kidneys, and brain, causing concern in humans, with indications of renal failure, anamia, and neurobehavioral changes described after high dosages.[11] Although Al can be absorbed through the skin and inhaled, the majority of Al organ load in the general population is caused by ingestion.[12] According to Al_2O_3-NPs' toxicokinetics and route of administration, these particles accumulate in the lungs and are then poured directly into the systemic circulatory blood, which carries them to various organs, including the thyroid and parathyroid glands, where they are accumulated and cause histopathological and physiological disorders.[13]

The antioxidant defense system in tissues is one of the body's natural defense mechanisms against free radicals.

Received: January 10, 2022
Accepted: April 7, 2022
Published: April 14, 2022

Curcumin (Cur), a significantly active turmeric compound with a wide range of biological and pharmacological effects, is one of the natural antioxidants.[14] N.Cur. is prepared to improve its aqueous-phase solubility and enhance permeability and delivery in circulation. Breaking Cur down to the nanosize has been shown in numerous trials to improve its bioavailability, large surface area, water solubility, unique drug delivery technology, and therapeutic efficacy.[15]

The antibacterial effect of N.Cur. has been reported to be more potent than that of the ordinary Cur, although they have the same chemical structure.[16] In addition, treatment with N.Cur. reduces the levels of the biomarkers of oxidative damage and increases the antioxidant content in the tissues.[17] Moreover, Cur inhibits tumor suppressor protein p53-related signaling pathways, promotes apoptosis of cancer cells by targeting mitochondria,[18] suppresses HepG2 cell growth and metastasis, and reduces the number of extracellular Hsp70.[19]

The present study aimed to compare the toxicity of Al_2O_3 and its NPs on hepatic and bone marrow tissues and to evaluate the efficacy of N.Cur. to protect hepatic and bone marrow cells from oxidative stress and apoptosis induced by Al_2O_3 and its NPs through relationships among Nrf2, Hsp70, and p53.

2. MATERIALS AND METHODS

2.1. Materials. Aluminum oxide (AL_2O_3) powder (Sigma-Aldrich) had the following characteristics: 99.99% trace metal basis, melting point/range: 2.040 °C, and initial boiling point and boiling range 2.980 °C, chemical stability stable under recommended storage condition. Pure Cur (Sigma-Aldrich) and aluminum oxide NPs were purchased from US Research Nanomaterials (Invitrogen, CA, USA). Sodium dodecyl-sulfate polyacrylamide gel electrophoresis (SDS-PAGE) chemicals, protease inhibitors, mouse anti-p53, anti-cleaved caspase-NRF-2, anti-Hsp70, goat anti-mouse immunoglobulin G (IgG)−horseradish peroxidase (HRP), goat anti-actin IgG, fetal bovine serum (USA), and GSH (Sigma-Aldrich) were used as obtained.

2.2. Ethical Approval. Adult male mice were kept in standard modes (temperature 25 ± 2 °C, lighting cycle 12 h light/dark, fed chow and water ad libitum) for 1 week to acclimatize prior to the commencement of the experiment. The research methodologies used in this study were examined and approved by the Medical Ethics Committee of the Molecular Biology Research Institute, Assiut University (no: IORG0010947-SCI-21-29-A), in accordance with the guidelines of the National Institutes of Health.

2.3. Experimental Design. Adult male mice (n = 72) weighing 22−26 g were divided into five groups: group 1 contained 12 mice, while the other four groups contained 15 mice each. Group I: served as the negative control (0.9% NaCl, 30% HCl 30% or 2% Tween-80); group II: served as the positive control treated with 6 mg/kg body weight (bw) of Al_2O_3[7] dissolved in HCl. Group (III): animals were treated with 6 mg/kg bw of Al_2O_3-NPs dissolved in 0.9% NaCl. Group IV: animals were treated with a combination of 6 mg/kg bw of Al_2O_3 and 20 mg/kg bw of N.Cur.[20] in 2% Tween-80. Group V: animals were treated with a combination of 6 mg/kg bw of Al_2O_3-NPs and 20 mg/kg bw of N.Cur. in 2% Tween-80. All treatments were administered orally for 4 weeks. Mice were anesthetized; blood was collected for the analysis of the complete blood count (CBC). Mice were dissected to obtain liver samples and bone marrow smear.

2.4. Characterization of Al_2O_3 and Al_2O_3-NPs. *2.4.1. X-ray Diffraction.* The crystal structures of powdered Al_2O_3 and Al_2O_3-NPs were studied at the Department of Physics, Faculty of Science, Assiut University, using a Philips X-ray diffractometer (model PW 1710, Holland).

2.4.2. Transmission Electron Microscopy and Stability. A drop of Al_2O_3 and Al_2O_3-NPs (20 nm/100 g/L) was released onto a carbon-coated copper grid and allowed to dry at room temperature. A transmission electron microscope was used to take micrographs of this sample at the Chemistry Department, Faculty of Science, Assiut University. The absorption spectra of the Al_2O_3-NPs were measured by UV−visible spectrophotometry (PG Instruments Limited, UK) at the beginning of the trial and before the water replacement (48 h).

2.4.3. Dynamic Light Scattering. The NPs' mean particle size and polydispersity index were measured at the International Center of Nanomedicine, Al-rajha Liver Hospital, Assiut University, using a Zetasizer Nano ZS instrument (Malvern Instruments, Worcestershire) equipped with a backscattered light detector operating at an angle of 173°. All samples were diluted in distilled water and measured in triplicate at 25 °C, and their volume was kept constant.

2.5. Preparation of Cur NPs and the Characterization Methods. Curcumin powder (100 mg) was dissolved in 20 mL dichloromethane to make a curcumin solution (5 mg/mL). Under ultrasonication conditions with a power and frequency of 50 kHz, 1 mL of the stock solution was introduced dropwise to boiling water (50 mL). For 30 min, the solution was sonicated. After sonication, the mixture was agitated for about 20 min at 800 rpm until an orange-colored precipitate was obtained. The supernatant was then discarded, and the pellet was employed for further biological study. A basic mixture of nanosuspension of 22.2% Cur in Tween 80 was used to test the samples, and the nanosuspension was kept in the dark and free of humidity.[16,21]

2.5.1. TEM and Optical Properties. The size and shape of the Cur-NLs were studied using transmission electron microscopy (TEM). A standard protocol was used to prepare the samples for TEM. The samples were air-dried before being examined under a transmission electron microscope. Optical characteristics were also determined through UV−visible spectroscopy analysis.[22]

2.5.2. Particle Size and Zeta Potential. The size and surface zeta potentials of N.Cur. were measured using a Malvern Zetasizer ZS (Zeta sizer nano-series Nano-s, Nawah Scientific, Egypt). Dynamic light scattering (DLS) and electrophoretic mobility testing were used to assess zeta potentials. Nanosuspension (4.5 mg) was solubilized in 10 mL deionized water and centrifuged at 5500 rpm for 20 min[23]

2.6. Western Blot. For immunoblot, RIPA was used to collect whole tissue lysates and electrophoresis on a 12% SDS-PAGE-separated 20 mg of protein, which was transferred onto a nitrocellulose membrane. After that, it was incubated on a non-fat dry milk in Tris-buffered saline. It was then treated with primary antibodies diluted in a blocking buffer. Finally, it was treated in a blocking buffer diluted with HRP-conjugated goat anti-rabbit IgG.[24] Using an image analyzer program, the absolute value of each band (concentration) was calculated using a densitometric activity.

2.7. Sodium Dodecyl-Sulfate Polyacrylamide Gel Electrophoresis. A 10% acrylamide resolving gel and a 3% acrylamide stacking gel SDS-PAGE sample buffer were used. A molecular weight standard (TaKaRa, Biotechnology, Dalian

https://doi.org/10.1021/acsomega.2c00195
ACS Omega 2022, 7, 13841−13852

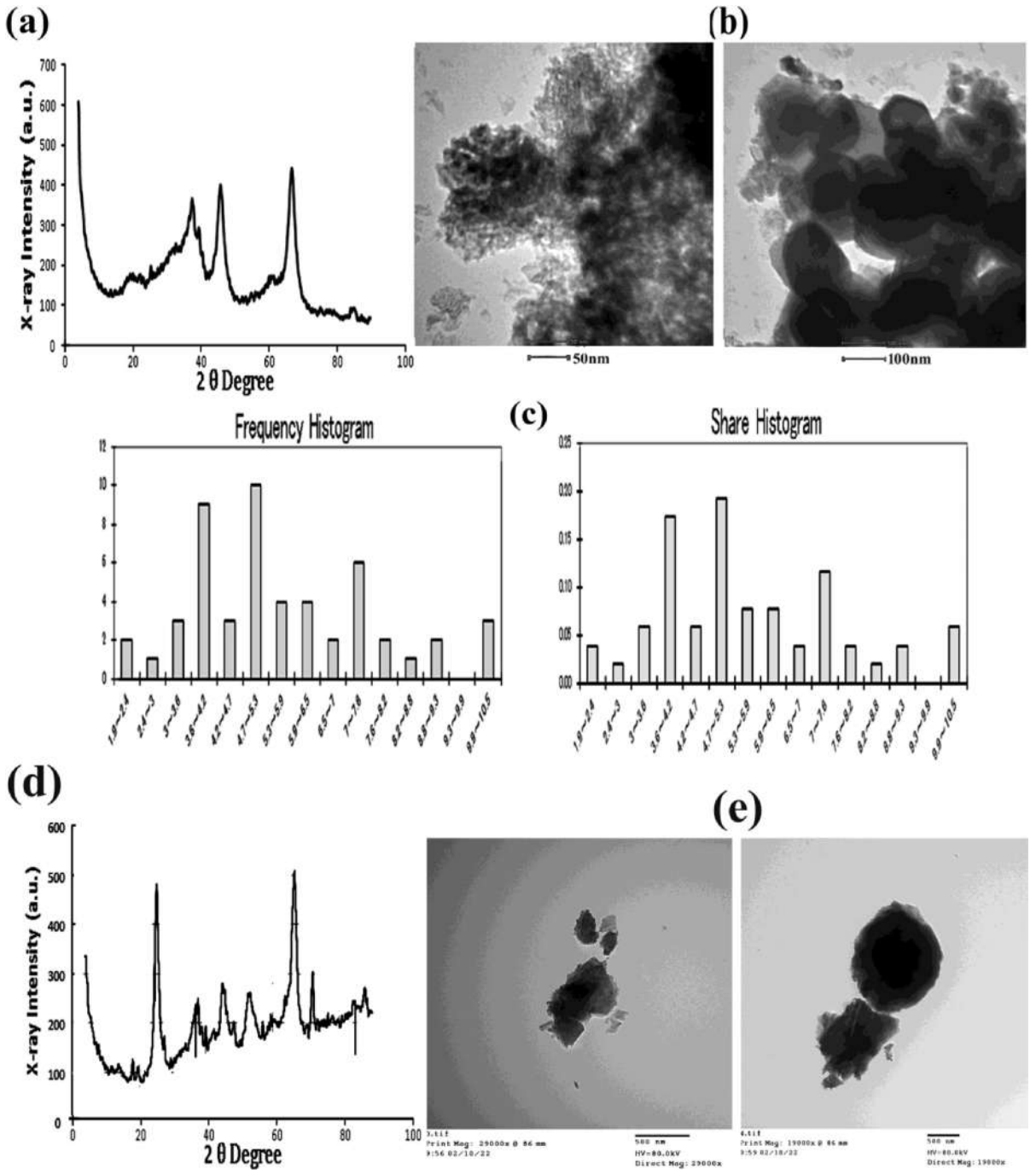

Figure 1. (a,d) XRD pattern analysis of Al_2O_3-NPs and Al_2O_3. (b,c,e) TEM and a histogram size distribution analysis of 20 nm/100 μg/L Al_2O_3-NPs and Al_2O_3 (bar = 50, 100, 500 nm).

Co., Ltd.) was also run, and serum protein bands were identified by comparing their electrophoretic patterns with standard markers.[25]

2.8. Bone Marrow Smearing and Count. Bone marrow is normally obtained from the femur, and the bone marrow smears were made traditionally. One method is to prepare bone marrow smears during necropsy and then use H and E staining to identify its cells and numbered in five fields on each of the three slides. The total number of bone marrow cells was counted by a hemocytometer and ImageJ software.[26]

2.9. Maturation Index Ratio and Complete Blood Count. The determination of the maturation index ratios (MIRs) for the numerical assessments of bone marrow cellularity was done by the following calculations: the ratio of myeloid to erythroid (M/E) is granulocytic and erythrocytic cell proportions. I/Mg: number of myeloblasts + promyelocytes + neutrophilic myelocytes/number of neutrophilic metamyelocytes, bands, and segmented neutrophils. MMI (1/I/Mg): number of neutrophilic metamyelocytes, bands, and segmented neutrophils/number of myeloblasts + promyelocytes + neutrophilic myelocytes. I/Me: number of proerythroblasts + basophilic erythroblasts/number of polychromatic and orthochromatic erythroblasts. EMI (1/I/Me): number of polychromatic and orthochromatic erythroblasts/number of proerythroblasts + basophilic erythroblasts.[27,28] CBC for 3 samples from each group was carried out by an Exigo

https://doi.org/10.1021/acsomega.2c00195
ACS Omega 2022, 7, 13841−13852

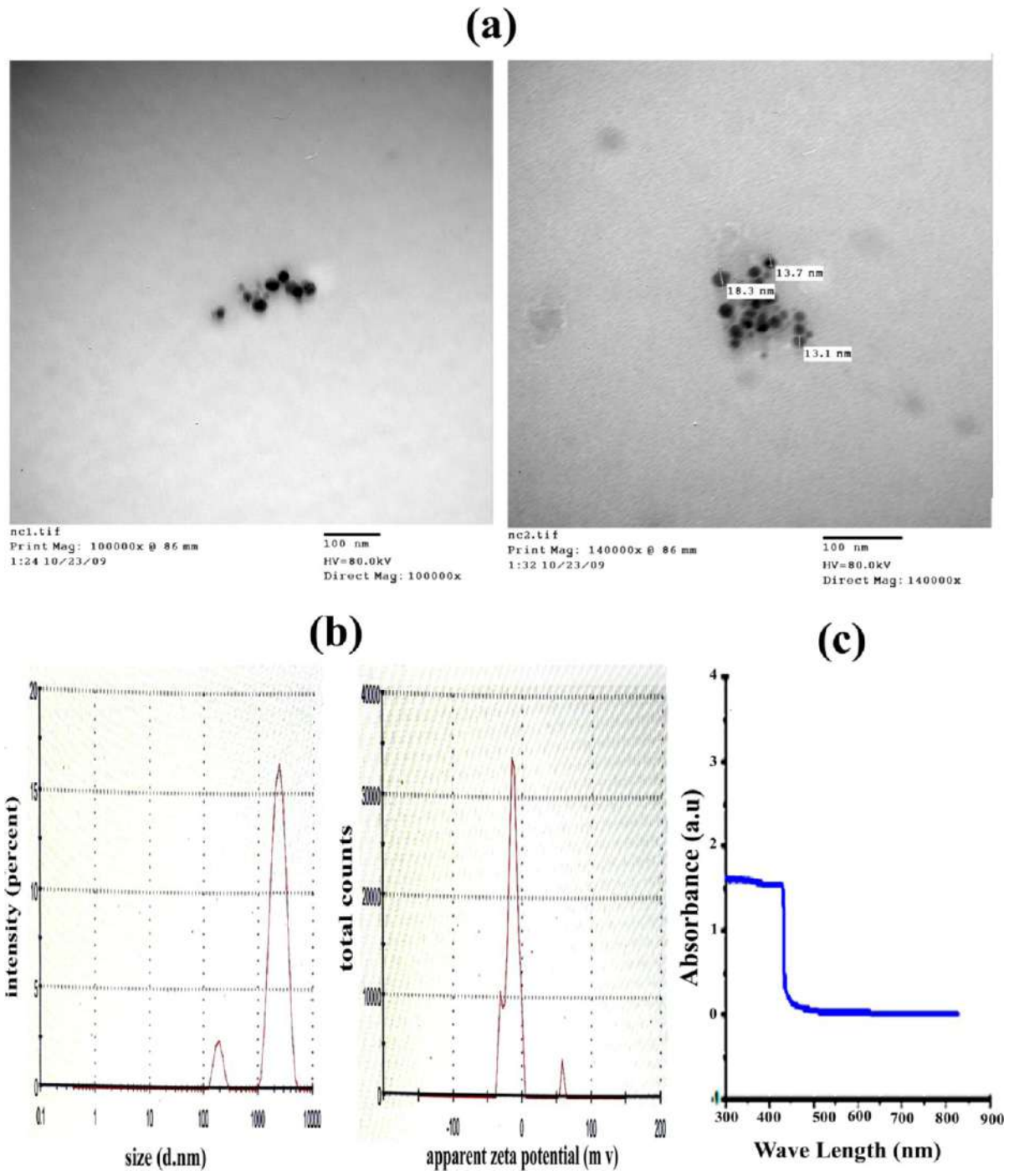

Figure 2. (a) TEM analysis of N.Cur. (bar = 100 nm). (b) Mean particle diameter, zeta potential measurements, and (c) optical absorption properties.

hematology analyzer at the Pathology Department, Faculty of Veterinary Medicine, Assiut University.

2.10. Histological and Histopathological Examination. Thick specimens (liver, 3−4 mm) were fixed in 10% neutral buffered formalin (pH 7.2), dried in gradient ethanol, and cleaned in xylene, and histological and histopathological tests were performed. After paraffin embedding, 3−5 μm sections were mounted on glass slides. Sections were deparaffinized twice in xylol for 30 min each time, then hydrated with an ethanol series before staining with hematoxylin and eosin and Masson trichrome as indicated. Five histopathological parameters were documented: region of degeneration, cytoplasmic color fading (light or heavy eosinophilic cytoplasm), nuclear condensation, nuclear fragmentation, and inflammation.[29] Collagenous fibers were examined at 40× in randomly chosen fields from at least three animals per group, and a fibrosis index (FI) was calculated as follows: FI = total positive area/total section area × 100.[30]

2.11. Statistical Analysis. The statistical significance of groups was determined by Student's *t*-test and one-way ANOVA ($P < 0.001$). All assays were performed in triplicate, and Graph Pad Prism 3 (Software Inc., USA) and ImageJ software were used.

https://doi.org/10.1021/acsomega.2c00195
ACS Omega 2022, 7, 13841−13852

3. RESULTS

3.1. Characterization of Al_2O_3-NPs and Al_2O_3. Analysis of Al_2O_3-NPs by X-ray diffraction (XRD) showed five dominant peak reflections corresponding to 20°(173), 38.54°(381), 45.26°(400), 67.72°(450), and 85.03°(99), which were observed on sets of lattice planes, as shown in Figure 1a. Micrographs of Al_2O_3-NPs obtained by TEM with their diameters (38.31 ± 2.45 nm, n = 60) and frequency of distributions are shown in Figure 1b,c. The absorption spectrum of the AL_2O_3-NPs was 20 nm/100 μg in the test solutions at 48 h (0.379 nm), which was higher than the absorption spectrum at the beginning of the trial (0.100 nm) at a wavelength of 380 nm. Moreover, DLS analysis of hydrodynamic diameter indicated that the NPs are bigger than those measured by micrographs obtained by TEM with the average size, by intensity, being 2257 ± 188.3 nm and the average particle size, by number, being 1577 ± 120.2 nm. Analysis of Al_2O_3 by XRD showed five dominant peak reflections corresponding to 20.5°(83), 25.42°(445), 38.5°(181), 44.92°(279), 54.94° (159), and 65.32°(278), which were observed on sets of lattice planes, as shown in Figure 1d. Micrographs of Al_2O_3 obtained by TEM are shown in Figure 1e.

Table 1. bw of Male Mice in Different Groups of the Experiment[a]

treatments	bw	% of change
control	26.53 ± 0.1878a	
Al_2O_3	25.96 ± 0.2554↓ab	2.15%
Al_2O_3NPs	23.57 ± 2.288↓b	11.15%
Al_2O_3 + N.Cur.	28.51 ± 0.2844↑a	7.46%
Al_2O_3NPs + N.Cur.	27.06 ± 0.2218↑a	1.9%

[a]Data are represented as mean ± SE. Changes in the mean values of proteins levels with different letters were significantly different (P < 0.001).

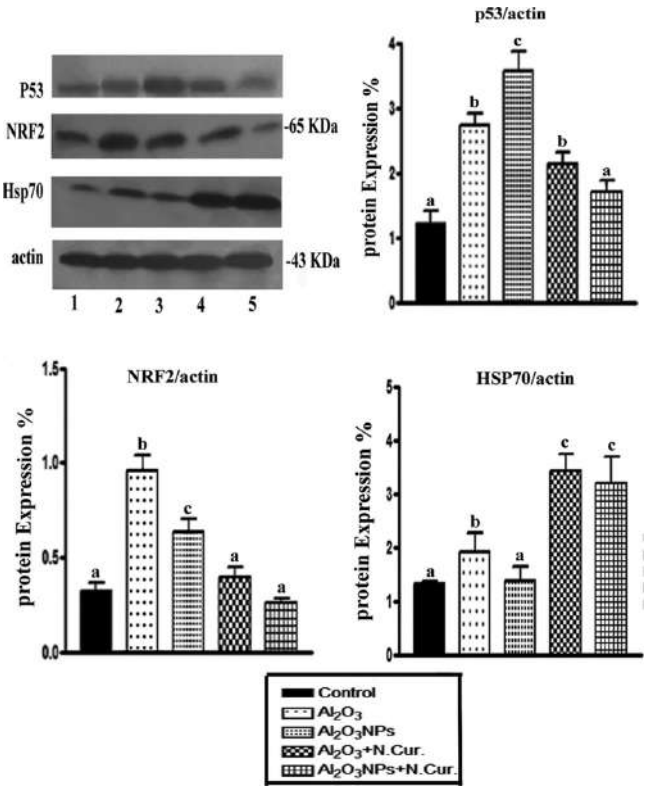

Figure 3. Immunoblot analysis was conducted to assess the effects of Al_2O_3 and Al_2O_3-NP exposure and various treatments on the protein levels of p53, Nrf2, and Hsp70. The percentage induction of protein/actin ratio after normalization to the control was calculated, and values with different letters were significant (P < 0.001).

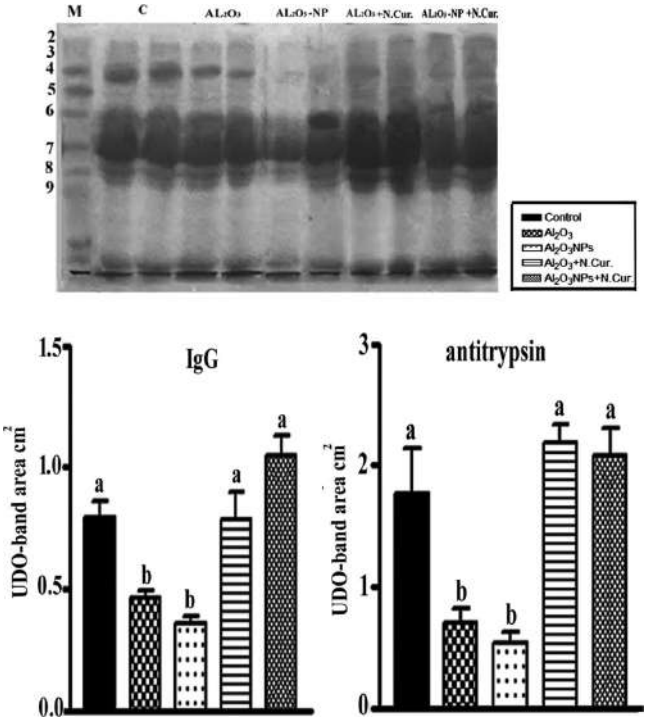

Figure 4. (a) SDS-PAGE estimation of serum protein fractions of control and different treatments, showing IgG and antitrypsin bands (4 and 8) and (168, and 60 KD), respectively. (b) Values with different letters were significant (P < 0.001).

3.2. Characterization of NPs of Cur (N.Cur.). N.Cur. have a globular form and varying sizes (<100 nm) as seen by TEM. Their frequency distributions are given in Figure 2a. The zeta-average size of N.Cur. was 1667, 1628, and 1548 (d·nm). The average particle size is bigger than that obtained from the transmission electron microscopic micrograph. The distribution report, by intensity, was 2123, 1991, and 2389 (d·nm). The zeta potential report was −14.2, −12.9, and −12.8 (mV), with the mean (mV) being −16.8, −13.6, and −17.7 and the area (%) being 78.9, 85.5, and 72.2, as shown in Figure 2b. UV−visible spectroscopy analysis of N.Cur. showed an absorption peak at 432 nm, as displayed in Figure 2c.

3.3. Body Weight. Table 1 shows the effect of AL_2O_3, AL_2O_3-NP, and nanocurcumin on bw gain or loss in mice when given singly or in combination. When compared to control animals, the difference in bw at the conclusion of the exposure was not statistically significant.

3.4. Western Blot Determination. The mice treated with Al_2O_3 and Al_2O_3-NPs exhibited a significant increase in the levels of p53 (125.62 and 200.00%, respectively) and Nrf2 (195.87 and 96.88%, respectively), but the level of Hsp70 was significantly decreased (46.15 and 6.9%, respectively) as compared with the control. Co-treatment of Al_2O_3 and Al_2O_3-NPs with N.Cur. caused a significant decrease in the level of p53 (21.98 and 59.37%, respectively) and Nrf2 (48.57 and 58.73%, respectively). In contrast, N.Cur. significantly

https://doi.org/10.1021/acsomega.2c00195
ACS Omega 2022, 7, 13841−13852

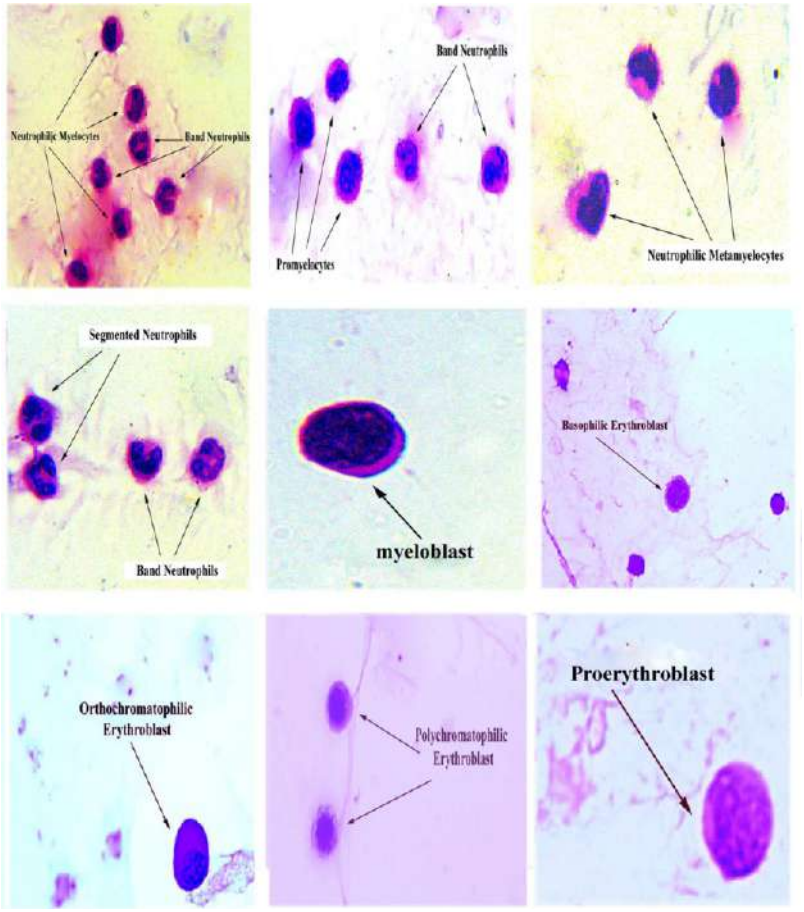

Figure 5. The high microscopic force of normal bone marrow smear shows various stages of maturing granulocytic cells and some of erythroid elements (X = 1000).

increased the levels of Hsp70 (84.21 and 137.41%, respectively) as compared with the untreated mice (Figure 3).

3.5. Measurements of IgG and Antitrypsin Levels. Al_2O_3 and Al_2O_3-NPs appeared to down-regulate the levels of IgG (42.01 and 362.30%) and antitrypsin (603.43, and 69.50%), respectively, compared to control mice. When Cur NPs were given to Al_2O_3- and Al_2O_3-NPs-treated mice, the previous proteins levels were increased by 71.02 and 32.64% for IgG and 68.59, and 287.39% for antitrypsin, respectively, versus those of Al_2O_3 and Al_2O_3-NPs groups (Figure 4).

3.6. Bone Marrow Estimation. *3.6.1. Morphology of Normal Bone Marrow Cells.* Examinations of bone marrow cells using a light microscope showed that myeloid cells have lighter staining nuclei and a pink cytoplasm. The myoblast was characterized by dispersed chromatin and granular cytoplasm. Promyelocytes had eccentric nuclei, prominent paranuclear space, and azurophilic granules. Neutrophilic myelocytes had rounded nucleus with a condensed chromatin and granular cytoplasm. Neutrophilic metamyelocytes had indented nuclei, a condensed chromatin, and a cytoplasm with secondary granules. Band neutrophil was characterized by a horseshoe-shaped mature nucleus and a cytoplasm with secondary granules. Segmented neutrophils had 3−5 discrete nuclear lobes and a highly condensed chromatin. The erythroid elements are smaller with rounded, dense, and deeply basophilic nuclei. The cytoplasm is basophilic in the blast form, with increase in eosinophilia as they mature (Figure 5).

3.6.2. Total and Differential Bone Marrow Cell Counts. The counts of various stages of some bone marrow cells, such as BMCs, myeloblasts, promyelocytes, neutrophilic myelocytes, neutrophilic metamyelocytes, segmented neutrophils, band neutrophils, proerythroblasts, basophilic erythroblasts, polychromatic erythroblasts, orthochromatic erythroblasts, and other cells were decreased in Al_2O_3- and Al_2O_3-NPs-treated groups than those of the control group. In N.Cur. co-treatment groups, the previous types of bone marrow counts were increased as compared with the Al_2O_3 and Al_2O_3-NPs groups. The mean values of the total count of bone marrow cells were 2800, 965, 851, 3000, and 2200 cells/10 μL in the control and different treatment groups. In addition, the percentages of differential bone marrow cell count were calculated as shown in Figure 6a,b.

3.6.3. MIR of Bone Marrow Cells. The present results revealed that the MIR of bone marrow cells was calculated in different treatments as shown in Table 2. This revealed that in the Al_2O_3 group, there was a significant increase in M/E, I/Mg, and EMI (1/I/Me) ratio index, while it significantly decreased ($P < 0.001$) in MMI (1/I/Mg) and I/Me as compared to the control group. In the Al_2O_3-NPs group, I/Mg and I/Me were significantly decreased and induced a significant increase in M/E, MMI, and EMI. It was found that in the Al_2O_3 and AL_2O_3-NPs co-treated with N.Cur. group, M/E, I/Mg, MMI (1/I/Mg), I/Me, and EMI (1/I/Me) were returned closely like the same index in the control group. According to CBC analysis, Al_2O_3 and Al_2O_3-NPs increased the total white blood cell

https://doi.org/10.1021/acsomega.2c00195
ACS Omega 2022, 7, 13841−13852

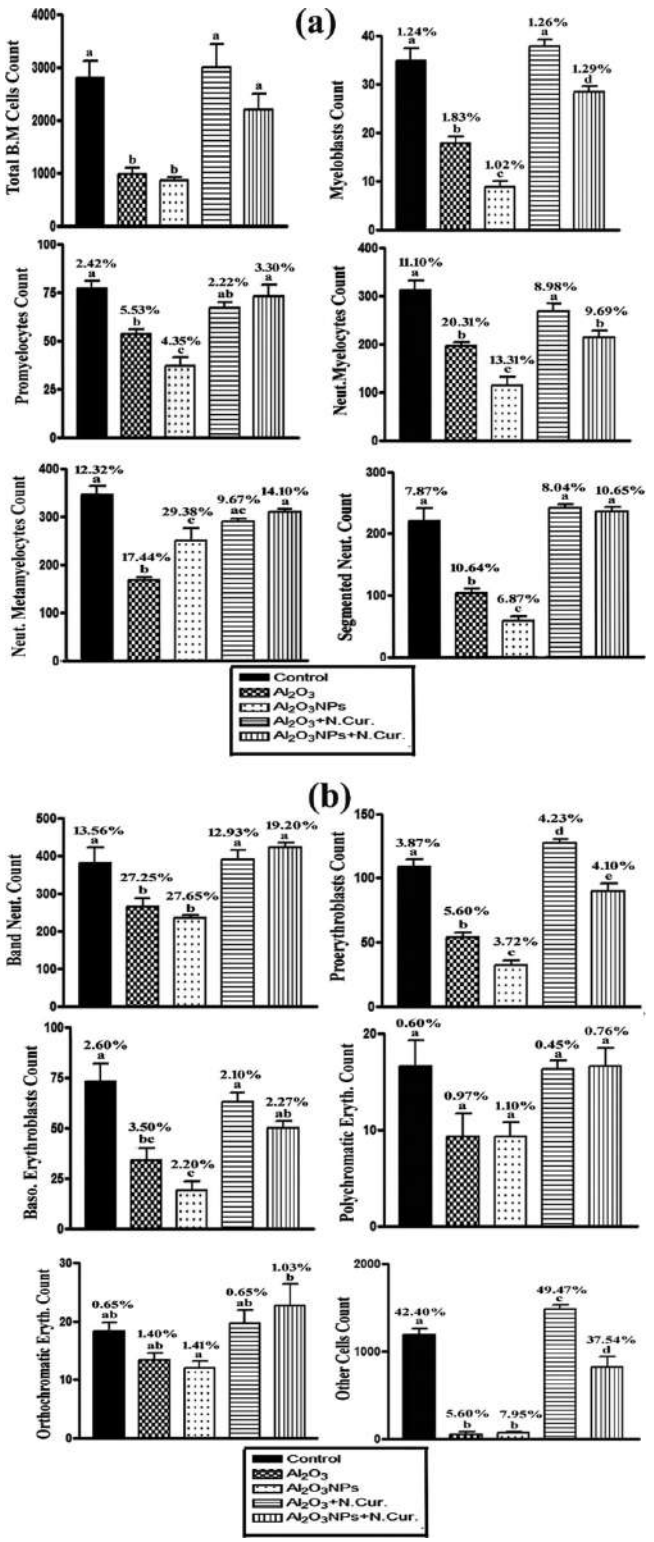

Figure 6. (a,b) Measurement of total and differential bone marrow cell counts in control and different treatments of male mice. The mean values with different letters are significant ($P < 0.001$).

count, but they decreased the red blood cell count in mice. Co-treatment with N.Cur. downregulated the WBC count and upregulated the red blood cell count (Table 3).

3.7. Histopathology and Liver Fibrosis Examination. Histologically, the liver sections from the control group showed normal architecture and distribution of collagen fibers in the liver (Figures 7a and 8a). In the Al_2O_3 group, the normal architecture of the liver structure was lost and there were massive cellular infiltrations and highly congested central veins (Figure 7b). In addition, there was an increase in the amounts of collagen fibers around the central vein and hepatocytes (Figure 8b). In the Al_2O_3-NP group, there was a great loss of the normal liver architecture, cellular infiltrations, congested central veins, and blood sinusoids with widespread necrotic cells (Figure 7c). There was also a massive increase in the collagen fibers (Figure 8c). The co-treatment of Al_2O_3 with N.Cur. resulted in the appearance of a nearly normal liver architecture and normal hepatocytes, but still some cellular infiltrations were present (Figure 7d) with moderate amounts of collagen fibers all over the parenchyma (Figure 8d). Furthermore, in the group co-treated with Al_2O_3-NPs and N.Cur., loss of normal architecture, congestion of the blood sinusoids, cellular infiltration, necrotic cells, and large amounts of collagen fibers were still present (Figures 7e and 8e). The histological score and liver fibrosis were higher in the Al_2O_3 and its NP groups (155, 175% and 75, 100%, respectively) as compared to the control group. The group that was treated with N.Cur. exhibited a substantial reduction in the score relative to the other groups (51, 54.5% and 42.1, 40%, respectively), as compared with the groups administered Al_2O_3 and its NPs (Figures 7f and 8f). Also, the present work showed that the treatment with Al_2O_3 and Al_2O_3-NPs increased plasma levels of AST and ALT with liver tissue damage compared to control. However, nanocurcumin administration reduced the previous liver function enzymes compared to treatment groups in male mice (Supporting Information).

Table 2. Bone Marrow Maturation Index Ratio (BMI) in Male Mice of Different Groups[a]

index ratio	M/E	I/Mg	MMI (I/I/Mg)	I/Me	EM1 (I/I/Me)
control	6.10	0.446	2.242	5.171	0.193
Al_2O_3	7.80	0.500	2.00	3.868	0.258
Al_2O_3-NPs	9.90	0.292	3.425	2.360	0.424
Al_2O_3 plus CUR-NPs	5.10	0.404	2.475	5.278	0189
Al_2O_3-NPs plus CUR-NPs	7.10	0.325	3.077	3.550	0.281

[a]Calculations of maturation index ratio; indicates M/E, M, myeloid; E, erythroid; I, immature; M, mature; I/Mg, immature/mature (granulopoiesis); MMI, myeloid maturation index; I/Me, immature/mature (erythropoiesis); EMI, erythroid maturation index.

4. DISCUSSION

In the present study, an analysis of Al_2O_3-NPs by TEM and DLS showed that NPs have average sizes of 38 nm and 2357 nm, respectively. However, Krause et al.[12] found that the core particle diameter of Al_2O_3 NPs was between 2 and 50 nm and it was rod-shaped as determined by TEM and 180 nm as determined by XRD. N.Cur. analysis showed that it was globular with various sizes (<1000 nm), and an absorption peak at 432 nm was observed based on the UV−visible spectroscopy analysis. In consistence, Pandit et al.[31] found that N.Cur. has an absorption peak range of 200−800 nm as detected by UV−visible spectroscopy and shows a spherical shape with polydisperse particles having the size range of 60−80 nm.

According to the current findings, Al_2O_3 and Al_2O_3-NPs impact hepatic tissues by boosting apoptosis through the activation of pro-apoptotic pathways via an increase in p53 and

https://doi.org/10.1021/acsomega.2c00195
ACS Omega 2022, 7, 13841−13852

Table 3. Effect of Al_2O_3 and Its NPs on Some CBC Parameters in Male Mice[a]

	control	Al_2O_3		Al_2O_3 NPs		Al_2O_3 + N.Cur.		Al_2O_3NPs + N.Cur.	
	mean ± SE	mean ± SE	% of change vs control	mean ± SE	% of change vs control	mean ± SE	% of change vs treat.	mean ± SE	% of change vs treat.
WBCs	6.7 ± 1.3a	7.7 ± 1.4 b↑	14.7%	9.1 ± 1.3c↑	37%	7.0 ± 1↓a	8.07% 22.9%	7.3 ± 1.0↓a	3.9% 19.5%
RBC	10.1 ± 0.5a	5.7 ± 0.3↓b	42.7%	7.5 ± 2.4↓b	26%	10 ± 1.2↑a	72.06% 32.41%	9.4 ± 1.2↑a	62.60% 25.12%

[a]Data are represented as mean ± SE. Changes in the mean values of proteins levels with different letters were significantly different ($P < 0.001$).

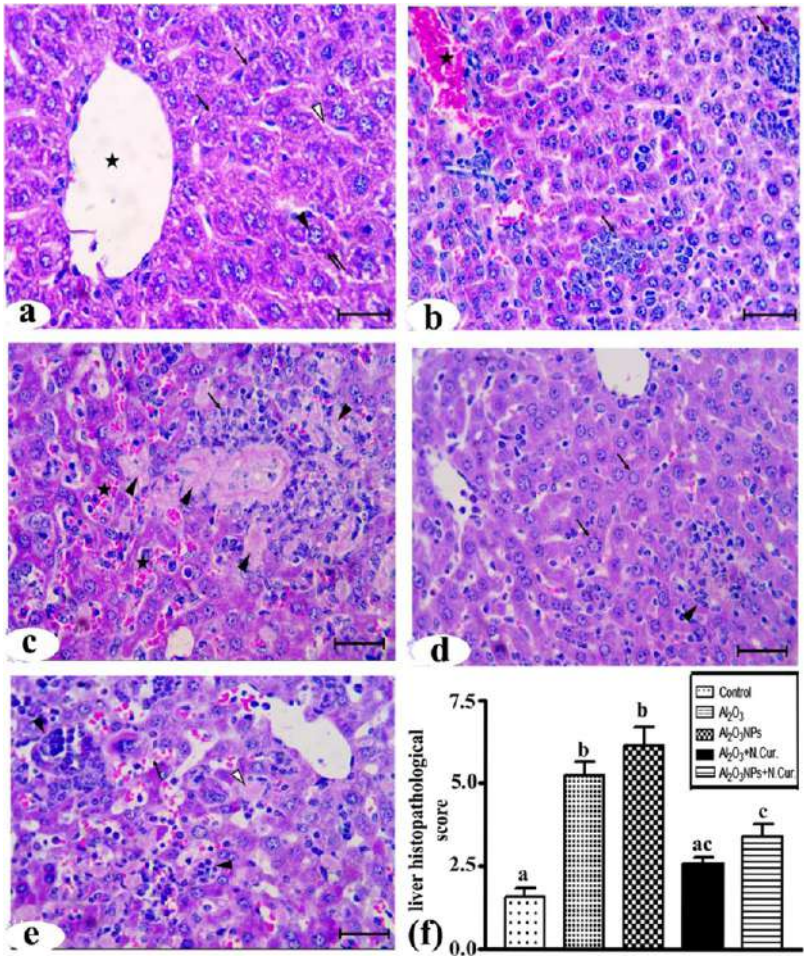

Figure 7. Photomicrographs of liver sections stained by HandE. (a) Control group showing central vein (*), normal hepatocytes (↑) with vesicular nuclei (▲), basophilic clumps (↑↑), and blood sinusoids (Δ). (b) Al_2O_3 group showing: massive cellular infiltrations (↑) and highly congested central vein (*). (c) Al_2O_3-NP group showing areas of necrosis (▲), cellular infiltrations (↑), and congested blood sinusoids (*). (d) Al_2O_3 + N.Cur. group showing nearly normal hepatocytes (↑) and some cellular infiltrations (▲). (e) Al_2O_3-NP + N.Cur. group showing congested blood sinusoids (↑), cellular infiltrations (▲), and necrotic cells (Δ) (bar = 50 μm). (f) liver histopathology scores of groups.

Nrf2 levels while lowering Hsp70 levels. Here, Al_2O_3-NPs caused a significant drop in Bcl-2 expression, while there was an increase in the p53 expression.[32] Additionally, it has been reported that the accumulation of Al_2O_3-NPs in the hippocampus of rats impacts the mitochondrial membrane's function and integrity of lipoproteins.[10]

NPs increased the production of ROS, which induced chromosomal damage and genotoxicity through primary signals of p53 expression.[33] Other findings of metal oxide NPs corroborated our findings, such as oxidative stress-mediated cytotoxicity and apoptotic response of bismuth oxide NPs in human breast cancer.[34] Nickel oxide NPs cause cytotoxicity and apoptosis in human liver cells via causing oxidative stress.[35] Mitochondrial-mediated apoptosis was induced in human hepatocarcinoma cells by copper oxide NPs.[36] MCF-7 and HT1080 cells have different cytotoxic and apoptotic responses to MnO_2 NPs, although they share a comparable method of action.[34]

The co-treatment with N.Cur. restored to the previous status and protected against oxidative stress that was induced by Al_2O_3 and its NPs. Similarly, M'rad et al. (2018)[37] found that Al-NPs caused toxicity and decrease in bw via increasing intracellular ROS levels. Moreover, Al_2O_3-NPs could induce oxidative stress via increased generation of ROS, which facilitates their transfer into other tissues through damage to cell membranes.[38] In vitro and in vivo studies on the cytotoxicity of Al NPs provided important insights into apoptosis and inflammatory effects by ROS that are induced

https://doi.org/10.1021/acsomega.2c00195
ACS Omega 2022, 7, 13841−13852

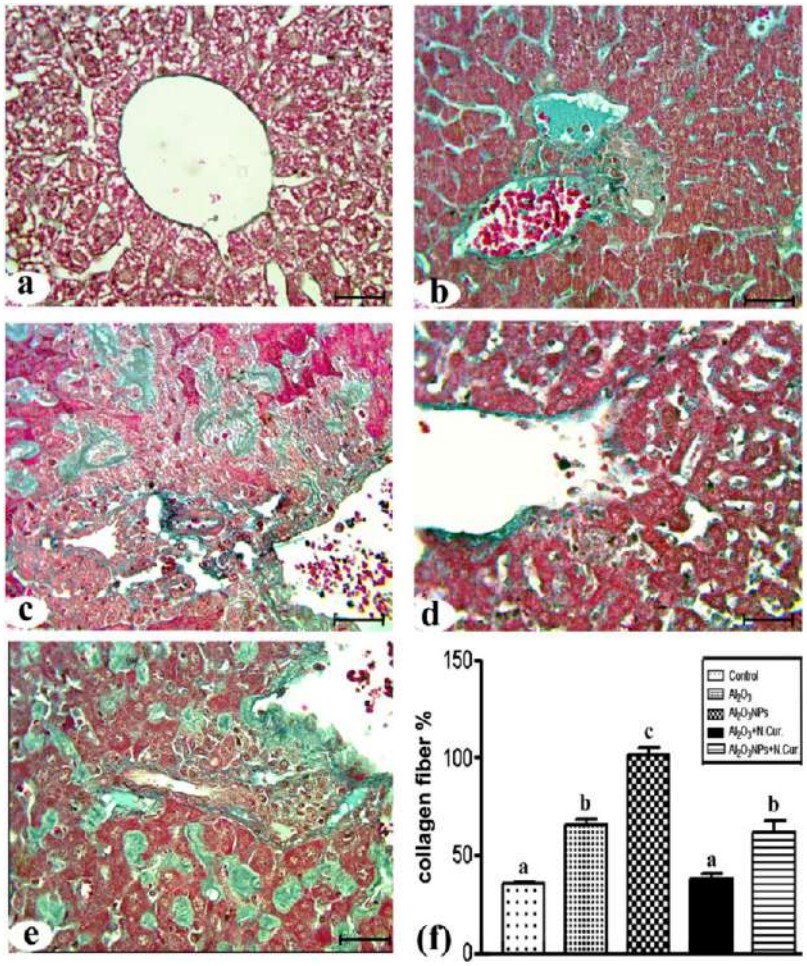

Figure 8. Photomicrographs of liver sections stained with Masson's trichrome stain. (a) Control group. (b) Al_2O_3 group showing an increase in the collagen fibers around central veins, sinusoids, and hepatocytes. (c) Al_2O_3-NP group showing a massive distribution of collagen fibers. (d) Al_2O_3 + N.Cur. group showing moderately distributed collagen fibers. (e) Al_2O_3-NP + N.Cur. group showing huge amounts of collagen fibers (bar = 50 μm). (f) The percentage of liver fibrosis.

by Al NPs.[39] Also, in cultured human cells, nickel oxide NPs cause cytotoxicity, oxidative stress, and apoptosis, which is inhibited by the dietary antioxidant curcumin.[40]

Our findings indicate that the oral intake of AL_2O_3-NP decreases bw and increases oxidative stress and toxicity, leading to apoptosis in the livers of mice, by the following mechanisms: (A) the regulation of P53 appears to be dependent on NRf2 and the level of Hsp70. (B) An increase in NRf2 is considered to be a non-defense system against oxidative stress, decreasing the endogenous antioxidant defense system and accelerating the increase in cytochrome *C*-induced apoptosis. Our findings demonstrated that oral supplementation with N.Cur. protects against hepatic apoptosis, which is manifested by down-regulation of p53 proteins.

This could be because Cur. induced the de novo synthesis of other proteins required for the stabilization of p53.[41] Furthermore, N.Cur. enhanced Nrf2 binding to the current AREs as a result of the inactivation of the Nrf2−Keap1 complex and the restoration of Nrf2 to a practically normal condition.[15] This is consistent with our findings because the toxicity of Al_2O_3 is associated with the overexpression of *Nrf2* gene, which impacted the Nrf2 signaling pathway. In addition, N.Cur. enhanced the endogenous defense systems in cells by regulating Nrf2 and scavenging hydrogen peroxide, hydroxyl radicals, and nitric oxide due to its phenolic and β-diketone functional groups.[42]

We observed that the co-treatment of mice with N.Cur. increased Hsp70 and lowered p53 activity, establishing a clear relationship between Hsp70 and apoptotic cell death. It is known that N.Cur. promotes Hsp70 overexpression and contributes to the prevention of cell death in HEI-193 cells.[43] Moreover, the overexpression of HspA1 in macrophages reduces cytochrome *C*, oxidative stress-induced apoptosis,[44] and caspase activation in U937 cells by preventing chromatin condensation.[45]

In this study, exposure to AL_2O_3 and its NPs increased liver fibrosis by decreasing antitrypsin and IgG in blood serum, resulting in excessive inflammatory activation, including a rise in the total white blood cells and a decrease in red blood cells. This revealed a relationship between antitrypsin and the systemic modulatory response.[46] Increased amounts of pro-fibrogenic chemicals, such as the transforming growth factor-β1 in mouse liver fibrosis, may be responsible for the activation of hepatic stellate cells.[47]

The exposure to Al_2O_3 and its NPs increased liver fibrosis and excessive inflammatory activation, including a rise in the total white blood cell count and a decrease in the red blood cell count. Furthermore, in the present study, we observed a decrease in the total and differential bone marrow cell count

https://doi.org/10.1021/acsomega.2c00195
ACS Omega 2022, 7, 13841−13852

with a change in the MIR in rats treated with Al_2O_3 and its NPs due to their myelotoxic effects that caused hypoplasia and apoptosis.[48] In the present study, the rise in the M/E ratio in the Al_2O_3-NPs group is connected with myeloid hyperplasia due to an increase in neutrophilic precursor cells, as evidenced by the rise in the I/Mg ratio. In dogs, after oxidative stress exposure, an increase in the M/E ratio is linked to myeloid hyperplasia associated with an increase in granulocytes, whereas a decrease in the M/E ratio is linked to erythroid hyperplasia caused by an increase in the erythropoietic series.[27]

Al NPs caused a disturbance in erythropoiesis and an increase in the white blood cell count[49] because NPs can travel through biological membranes and into the cytoplasm and nucleus of cells. In the present work, N.Cur. restored the MIR in bone marrow and the total erythrocyte and leukocyte count close to the normal levels, indicating the ability of N.Cur. to protect from the toxicity associated with NPs due to the NP's extended duration of circulation in the blood and the increase in its bioavailability.[50] Curcumin NPs have demonstrated their ability to act as a free-radical scavenger and to reduce heavy metal toxicity. Due to their small particle size, these particles are easily accessible in the body and can be transported to various body sites via blood circulation.[50]

Histopathological observations showed that the oral administration of Al_2O_3 and its NPs induced congestion of blood sinusoids, inflammation, fibrosis, and necrosis of the hepatocytes. Similar pathological changes in the liver, testes, and kidneys after oral exposure to Al_2O_3 were reported by Hadi and Jaffat (2016).[51] The observed hepatic necrosis and disarray along with the cell−cell dissociation could be ascribed to the overproduction of ROS induced by Al NPs.[52] Also, our findings are in line with those of Canli et al. (2019),[8] who reported on the histological effects of NPs of metallic oxides on liver samples of rats. However, the present work found that N.Cur. improved the pathological changes and oxidative stress status due to an upregulation in GSH levels by controlling its expression levels through binding to the antioxidant response element in the promoters of Nrf2-regulated phase II detoxifying enzymes.[53] Also, the bioavailability and controlled release of nanocurcumin could be responsible for increased cellular immune responses.[54]

5. CONCLUSIONS

Nanocurcumin is a potent free radical quencher with antioxidant properties. It effectively mitigates and inhibits the harmful effects and oxidative stress caused by Al_2O_3 and Al_2O_3-NPs in the blood, bone marrow, and liver samples of mice. In addition, the regulation of Hsp70 appears to be dependent on NRf2 and the levels of p53. An increase in NRf2 levels is considered to be a defense system against oxidative stress.

■ ASSOCIATED CONTENT

Supporting Information

The Supporting Information is available free of charge at https://pubs.acs.org/doi/10.1021/acsomega.2c00195.

Effect of Al_2O_3, Al_2O_3NPs, and N.Cur. on plasma activities of liver functions, AST, and ALT in male mice (PDF)

■ AUTHOR INFORMATION

Corresponding Author

Mona M. Atia − *Laboratory of Molecular Cell Biology; Department of Zoology, Faculty of Science, Assiut University, Assiut 71515, Egypt;* orcid.org/0000-0002-0660-0985; Email: monatia@aun.edu.eg

Authors

Alshaimaa A. I. Alghriany − *Laboratory of Molecular Cell Biology; Department of Zoology, Faculty of Science, Assiut University, Assiut 71515, Egypt;* orcid.org/0000-0003-0970-3653

Hossam EL-din M. Omar − *Laboratory of Physiology, Department of Zoology, Faculty of Science, Assiut University, Assiut 71515, Egypt;* orcid.org/0000-0002-1456-0506

Amera M. Mahmoud − *Laboratory of Physiology, Department of Zoology, Faculty of Science, Assiut University, Assiut 71515, Egypt;* orcid.org/0000-0002-9656-5027

Complete contact information is available at: https://pubs.acs.org/10.1021/acsomega.2c00195

Notes

The authors declare no competing financial interest.

■ ACKNOWLEDGMENTS

This work was facilitated by the Laboratory of Molecular Cell Biology of the Zoology Department of the Faculty of Science, Assiut University, Egypt.

■ ABBREVIATIONS

Al_2O_3-NPs, aluminum oxide nanoparticles; ROS, reactive oxygen species; N-Cur, nanocurcumin; MIRmaturation index ratioEGTA, maturation index ratioEGTAethylene glycol tetra-acetic acid; TEM, transmission electron microscopy; HSP70, heat shock proteins; Nrf2, nuclear factor erythroid 2-related factor 2

■ REFERENCES

(1) Vignal, C.; Desreumaux, P.; Body-Malapel, M. Gut: An underestimated target organ for Aluminum. *Morphologie* **2016**, *100*, 75−84.

(2) Gehrke, I.; Geiser, A.; Somborn-Schulz, A. Innovations in nanotechnology for water treatment. *Nanotechnol., Sci. Appl.* **2015**, *8*, 1.

(3) Modena, M. M.; Rühle, B.; Burg, T. P.; Wuttke, S. Nanoparticle characterization: what to measure? *Adv. Mater.* **2019**, *31*, 1901556.

(4) Li, N.; Xia, T.; Nel, A. E. The role of oxidative stress in ambient particulate matter-induced lung diseases and its implications in the toxicity of engineered nanoparticles. *Free Radicals Biol. Med.* **2008**, *44*, 1689−1699.

(5) Willhite, C. C.; Karyakina, N. A.; Yokel, R. A.; Yenugadhati, N.; Wisniewski, T. M.; Arnold, I. M. F.; Momoli, F.; Krewski, D. Systematic review of potential health risks posed by pharmaceutical, occupational and consumer exposures to metallic and nanoscale aluminum, aluminum oxides, aluminum hydroxide and its soluble salts. *Crit. Rev. Toxicol.* **2014**, *44*, 1−80.

(6) Geraets, L.; Oomen, A. G.; Krystek, P.; Jacobsen, N. R.; Wallin, H.; Laurentie, M.; Verharen, H. W.; Brandon, E. F.; de Jong, W. H. Tissue distribution and elimination after oral and intravenous administration of different titanium dioxide nanoparticles in rats. *Part. Fibre Toxicol.* **2014**, *11*, 30.

(7) Park, E.-J.; Sim, J.; Kim, Y.; Han, B. S.; Yoon, C.; Lee, S.; Cho, M.-H.; Lee, B.-S.; Kim, J.-H. A 13-week repeated-dose oral toxicity and bioaccumulation of aluminum oxide nanoparticles in mice. *Arch. Toxicol.* **2015**, *89*, 371.

(8) Canli, E. G.; Ila, H. B.; Canli, M. Response of the antioxidant enzymes of rats following oral administration of metal-oxide nanoparticles (Al_2O_3, CuO, TiO_2). *Environ. Sci. Pollut. Res.* **2019**, *26*, 938−945.
(9) Kim, Y.-S.; Chung, Y.-H.; Seo, D.-S.; Choi, H.-S.; Lim, C.-H. Twenty-eight-day repeated inhalation toxicity study of aluminum oxide nanoparticles in male Sprague-Dawley rats. *Toxicol. Res.* **2018**, *34*, 343−354.
(10) Yousef, M. I.; Mutar, T. F.; Kamel, M. A. E.-N. Hepato-renal toxicity of oral sub-chronic exposure to aluminum oxide and/or zinc oxide nanoparticles in rats. *Toxicol. Rep.* **2019**, *6*, 336−346.
(11) Krewski, D.; Yokel, R. A.; Nieboer, E.; Borchelt, D.; Cohen, J.; Harry, J.; Kacew, S.; Lindsay, J.; Mahfouz, A. M.; Rondeau, V. Human health risk assessment for aluminium, aluminium oxide, and aluminium hydroxide. *J. Toxicol. Environ. Health, Part B* **2007**, *10*, 1−269.
(12) Krause, B. C.; Kriegel, F. L.; Rosenkranz, D.; Dreiack, N.; Tentschert, J.; Jungnickel, H.; Jalili, P.; Fessard, V.; Laux, P.; Luch, A. Aluminum and aluminum oxide nanomaterials uptake after oral exposure—a comparative study. *Sci. Rep.* **2020**, *10*, 2698.
(13) Morsy, G. M.; Abou El-Ala, K. S.; Ali, A. A. Studies on fate and toxicity of nanoalumina in male albino rats. *Toxicol. Ind. Health* **2016**, *32*, 200−214.
(14) Fakhri, S.; Shakeryan, S.; Alizadeh, A.; Shahryari, A. Effect of 6 Weeks of High Intensity Interval Training with Nano curcumin Supplement on Antioxidant Defense and Lipid Peroxidation in Overweight Girls- Clinical Trial. *Iran. J. diabetes Obes.* **2020**, *11*, 173.
(15) Sookhaklari, R.; Geramizadeh, B.; Abkar, M.; Moosavi, M. The neuroprotective effect of BSA-based nanocurcumin against 6-OHDA-induced cell death in SH-SY5Y cells. *Avicenna J. Phytomed.* **2019**, *9*, 92.
(16) Carvalho, D. d. M.; Takeuchi, K. P.; Geraldine, R. M.; Moura, C. J. d.; Torres, M. C. L. Production, solubility and antioxidant activity of curcumin nanosuspension. *Food Sci. Technol.* **2015**, *35*, 115−119.
(17) Abdel-Wahhab, M. A.; Ismaiel, A. A.; El-Denshary, E. S.; El-Nekeety, A. A.; Al-Yamani, A. F.; Gad, S. A.; Hassan, N. S. Ameliorative effects of curcumin nanoparticles on hepatotoxicity induced by zearalenone mycotoxin. *Global J. Pharmacol.* **2015**, *9*, 234−245.
(18) Shankar, S.; Srivastava, R. Involvement of Bcl-2 family members, phosphatidylinositol 3'-kinase/AKT and mitochondrial p53 in curcumin (diferulolylmethane)-induced apoptosis in prostate cancer. *Int. J. Oncol.* **2007**, *30*, 905−918.
(19) Ren, B.; Luo, S.; Tian, X.; Jiang, Z.; Zou, G.; Xu, F.; Yin, T.; Huang, Y.; Liu, J. Curcumin inhibits liver cancer by inhibiting DAMP molecule HSP70 and TLR4 signaling. *Oncol. Rep.* **2018**, *40*, 895−901.
(20) Hassan, S. K.; Mousa, A. M.; Eshak, M. G.; Farrag, A.; Badawi, A. Therapeutic and chemopreventive effects of nano curcumin against diethylnitrosamine induced hepatocellular carcinoma in rats. *Int. J. Pharm. Pharm. Sci.* **2014**, *6*, 54−62.
(21) Mohamed Ibrahim, R.; El Zahraa Ali Abd Elaal, F.; Zaki, S. Effect of Curcumin and Nano-curcumin on Reduce Aluminum Toxicity in Rats. *Int. J. Food Sci. Bioechnol* **2019**, *4*, 64.
(22) Bhawana, R. K.; Basniwal, R. K.; Buttar, H. S.; Jain, V. K.; Jain, N. Curcumin nanoparticles: preparation, characterization, and antimicrobial study. *J. Agric. Food Chem.* **2011**, *59*, 2056−2061.
(23) Hanna, D. H.; Saad, G. R. Nanocurcumin: preparation, characterization and cytotoxic effects towards human laryngeal cancer cells. *RSC Adv.* **2020**, *10*, 20724−20737.
(24) Seo, S. U.; Min, K.-j.; Woo, S. M.; Kwon, T. K. Z-FL-COCHO, a cathepsin S inhibitor, enhances oxaliplatin-mediated apoptosis through the induction of endoplasmic reticulum stress. *Exp. Mol. Med.* **2018**, *50*, 1−11.
(25) Partovi, R.; Seifi, S.; Pabast, M.; Babaei, A. Effects of dietary supplementation with nanocurcumin on quality and safety of meat from broiler chicken infected with Eimeria species. *J. Food Saf.* **2019**, *39*, No. e12703.
(26) Mischke, R.; Busse, L. Reference values for the bone marrow aspirates in adult dogs. *J. Vet. Med. Ser. A* **2002**, *49*, 499−502.
(27) Trópia de Abreu, R.; Carvalho, M. D. G.; Carneiro, C. M.; Giunchetti, R. C.; Teixeira-Carvalho, A.; Martins-Filho, O. A.; et al. Influence of clinical status and parasite load on erythropoiesis and leucopoiesis in dogs naturally infected with Leishmania (Leishmania) chagasi. *PLoS One* **2011**, *6*, No. e18873.
(28) Elmore, S. A. Enhanced histopathology of the bone marrow. *Toxicol. Pathol.* **2006**, *34*, 666−686.
(29) Heijnen, B. H. M.; Straatsburg, I. H.; Gouma, D. J.; van Gulik, T. M. Decrease in core liver temperature with 10°C by in situ hypothermic perfusion under total hepatic vascular exclusion reduces liver ischemia and reperfusion injury during partial hepatectomy in pigs. *Surgery* **2003**, *134*, 806−817.
(30) Bataller, R.; Schwabe, R. F.; Choi, Y. H.; Yang, L.; Paik, Y. H.; Lindquist, J.; Qian, T.; Schoonhoven, R.; Hagedorn, C. H.; Lemasters, J. J.; et al. NADPH oxidase signal transduces angiotensin II in hepatic stellate cells and is critical in hepatic fibrosis. *J. Clin. Invest.* **2003**, *112*, 1383−1394.
(31) Pandit, R. S.; Gaikwad, S. C.; Agarkar, G. A.; Gade, A. K.; Rai, M. Curcumin nanoparticles: physico-chemical fabrication and its in vitro efficacy against human pathogens. *3 Biotech* **2015**, *5*, 991−997.
(32) Liu, H.; Zhang, W.; Fang, Y.; Yang, H.; Tian, L.; Li, K.; Lai, W.; Bian, L.; Lin, B.; Liu, X.; et al. Neurotoxicity of aluminum oxide nanoparticles and their mechanistic role in dopaminergic neuron injury involving p53-related pathways. *J. Hazard. Mater.* **2020**, *392*, 122312.
(33) Rajiv, S.; Jerobin, J.; Saranya, V.; Nainawat, M.; Sharma, A.; Makwana, P.; Gayathri, C.; Bharath, L.; Singh, M.; Kumar, M.; et al. Comparative cytotoxicity and genotoxicity of cobalt (II, III) oxide, iron (III) oxide, silicon dioxide, and aluminum oxide nanoparticles on human lymphocytes in vitro. *Hum. Exp. Toxicol.* **2016**, *35*, 170−183.
(34) Alhadlaq, H. A.; Akhtar, M. J.; Ahamed, M. Different cytotoxic and apoptotic responses of MCF-7 and HT1080 cells to MnO2 nanoparticles are based on similar mode of action. *Toxicology* **2019**, *411*, 71−80.
(35) Ahamed, M.; Ali, D.; Alhadlaq, H. A.; Akhtar, M. J. Nickel oxide nanoparticles exert cytotoxicity via oxidative stress and induce apoptotic response in human liver cells (HepG2). *Chemosphere* **2013**, *93*, 2514−2522.
(36) Siddiqui, M. A.; Alhadlaq, H. A.; Ahmad, J.; Al-Khedhairy, A. A.; Musarrat, J.; Ahamed, M. Copper oxide nanoparticles induced mitochondria mediated apoptosis in human hepatocarcinoma cells. *PLoS One* **2013**, *8*, No. e69534.
(37) M'rad, I.; Jeljeli, M.; Rihane, N.; Hilber, P.; Sakly, M.; Amara, S. Aluminium oxide nanoparticles compromise spatial learning and memory performance in rats. *EXCLI J.* **2018**, *17*, 200.
(38) Prabhakar, P. V.; Reddy, U. A.; Singh, S. P.; Balasubramanyam, A.; Rahman, M. F.; Indu Kumari, S.; Agawane, S. B.; Murty, U. S. N.; Grover, P.; Mahboob, M. Oxidative stress induced by aluminum oxide nanomaterials after acute oral treatment in Wistar rats. *J. Appl. Toxicol.* **2012**, *32*, 436−445.
(39) Abbas, O. A.; Ibrahim, I. G.; Ismail, A.-G. E. Therapeutic effects of nano-hap in a rat model of alcl3 induced neurotoxicity. *Iran. J. Pharm. Res.* **2019**, *18*, 1309−1322.
(40) Siddiqui, M. A.; Ahamed, M.; Ahmad, J.; Khan, M. A. M.; Musarrat, J.; Al-Khedhairy, A. A.; Alrokayan, S. A. Nickel oxide nanoparticles induce cytotoxicity, oxidative stress and apoptosis in cultured human cells that is abrogated by the dietary antioxidant curcumin. *Food Chem. Toxicol.* **2012**, *50*, 641−647.
(41) Sa, G.; Das, T. Anti cancer effects of curcumin: cycle of life and death. *Cell Div.* **2008**, *3*, 14.
(42) Silva, L. S. D.; Catalão, C. H. R.; Felippotti, T. T.; Oliveira-Pelegrin, G. R. D.; Petenusci, S.; de Freitas, L. A. P.; Rocha, M. J. A. Curcumin suppresses inflammatory cytokines and heat shock protein 70 release and improves metabolic parameters during experimental sepsis. *Pharm. Biol.* **2017**, *55*, 269−276.
(43) Angelo, L. S.; Wu, J. Y.; Meng, F.; Sun, M.; Kopetz, S.; McCutcheon, I. E.; Slopis, J. M.; Kurzrock, R. Combining curcumin

https://doi.org/10.1021/acsomega.2c00195
ACS Omega 2022, 7, 13841−13852

(diferuloylmethane) and heat shock protein inhibition for neurofibromatosis 2 treatment: analysis of response and resistance pathways. *Mol. Cancer Ther.* **2011**, *10*, 2094−2103.
(44) Klein, S. D.; Brüne, B. Heat-shock protein 70 attenuates nitric oxide-induced apoptosis in RAW macrophages by preventing cytochrome c release. *Biochem. J.* **2002**, *362*, 635−641.
(45) Chatterjee, S.; Burns, T. Targeting heat shock proteins in cancer: a promising therapeutic approach. *Int. J. Mol. Sci.* **2017**, *18*, 1978.
(46) Bergin, D. A.; Hurley, K.; McElvaney, N. G.; Reeves, E. P. Alpha-1 antitrypsin: a potent anti-inflammatory and potential novel therapeutic agent. *Arch. Immunol. Ther. Exp.* **2012**, *60*, 81−97.
(47) Cheng, Y.; Luo, R.; Zheng, H.; Wang, B.; Liu, Y.; Liu, D.; Chen, J.; Xu, W.; Li, A.; Zhu, Y. Synergistic anti-tumor efficacy of sorafenib and fluvastatin in hepatocellular carcinoma. *Oncotarget* **2017**, *8*, 23265.
(48) Jalili, P.; Huet, S.; Lanceleur, R.; Jarry, G.; Hegarat, L. L.; Nesslany, F.; Hogeveen, K.; Fessard, V. Genotoxicity of aluminum and aluminum oxide nanomaterials in rats following oral exposure. *Nanomaterials* **2020**, *10*, 305.
(49) Kahbasi, S.; Samadbin, M.; Attar, F.; Heshmati, M.; Danaei, D.; Rasti, B.; Salihi, A.; Nanakali, N. M. Q.; Aziz, F. M.; Akhtari, K.; et al. The effect of aluminum oxide on red blood cell integrity and hemoglobin structure at nanoscale. *Int. J. Biol. Macromol.* **2019**, *138*, 800−809.
(50) Yadav, A.; Flora, S. J. S.; Kushwaha, P. Nanocurcumin prevents oxidative stress induced following arsenic and fluoride co-exposure in rats. *Def Life Sci J* **2016**, *1*, 69−77.
(51) Hadi, A.-H. A.; Jaffat, H. S. Effect of aluminum-containing antacid on sperm parameters and testicular structure in male rats. *Int. J. PharmTech Res.* **2016**, *9*, 267−271.
(52) Siddique, N. A.; Mujeeb, M.; Najmi, A. K.; Aftab, A.; Aslam, J. Free radical scavenging and hepatoprotective activity of Aegle marmelos (linn.) corr leaves against carbon tetrachloride. *Int. J. Compr. Pharm.* **2011**, *2*, 1−6.
(53) Estakhri, M. A.; Shokrzadeh, M.; Jaafari, M. R.; Karami, M.; Mohammadi, H. Organ toxicity attenuation by nanomicelles containing curcuminoids: Comparing the protective effects on tissues oxidative damage induced by diazinon. *Iran. J. Basic Med. Sci.* **2019**, *22*, 17.
(54) Afolayan, F. I. D.; Erinwusi, B.; Oyeyemi, O. T. Immunomodulatory activity of curcumin-entrapped poly d,l -lactic-co -glycolic acid nanoparticles in mice. *Integr. Med. Res.* **2018**, *7*, 168−175.

https://doi.org/10.1021/acsomega.2c00195
ACS Omega 2022, 7, 13841−13852